

Absolute calibration of a wideband antenna and spectrometer for accurate sky noise temperature measurements

Alan E. E. Rogers¹ and Judd D. Bowman²

Received 5 December 2011; revised 11 May 2012; accepted 25 May 2012; published 4 July 2012.

[1] A new method of absolute calibration of sky noise temperature using a three-position switched spectrometer, measurements of antenna and low noise amplifier impedance with a vector network analyzer, and ancillary measurements of the amplifier noise waves is described and compared with other methods of calibration. An initial test of the method has been made using brief observations from 55 to 110 MHz at West Forks, Maine, to estimate the sky noise spectral index. Estimates are made of the accuracy that might ultimately be achieved with observations to detect or set limits on the red-shifted 21 cm line at a radio quiet site. It is concluded that an antenna reflection coefficient better than about -20 dB is required to avoid being limited by the accuracy of the antenna reflection coefficient measurements using a vector network analyzer.

Citation: Rogers, A. E. E., and J. D. Bowman (2012), Absolute calibration of a wideband antenna and spectrometer for accurate sky noise temperature measurements, *Radio Sci.*, 47, RS0K06, doi:10.1029/2011RS004962.

1. Introduction

[2] Accurately calibrated sky noise observations are needed to measure the spectral index of the diffuse radio background which is important in determining the emission mechanisms in the Galactic and extragalactic background. Theoretical models of the early universe predict small deviations in the spectrum of the radio sky due to emission and absorption of neutral hydrogen at redshifts which place the 21 cm line in the 50–200 MHz range [Shaver *et al.*, 1999; Gnedin and Shaver, 2004; Furlanetto *et al.*, 2006]. In addition to the applications in radio astronomy, accurately calibrated sky noise measurements are used to measure the absorption of radio signals in the ionosphere using riometers [Hargreaves and Detrick, 2002]. Also, accurate calibration has applications in antenna pattern measurements and spectrum monitoring.

[3] The measurement of the antenna temperature is affected by the antenna impedance as any mismatch to the receiver results in a fraction of the sky noise power, T_{sky} , being reflected back into the sky so that the measured noise temperature from the antenna, T_{ant} , is

$$T_{ant} = T_{sky}(1 - |\Gamma|^2) \quad (1)$$

where Γ is the reflection coefficient. In addition outgoing noise from the receiver is reflected back to the receiver by

the mismatch. The “mismatch” can be corrected by using a mechanical tuner to adjust the antenna impedance to obtain the same impedance as the calibrated noise source used to calibrate the receiver. Under this condition any power lost due to the Low Noise Amplifier (LNA) having a different impedance is the same for the antenna as it is for the noise source. Several accurately calibrated measurements of the sky noise spectral index using this method were published in the 1960s and 1970s [Pauliny-Toth and Shakeshaft, 1962; Turtle *et al.*, 1962]. However, this method is limited to a narrow frequency range and requires constructing scaled antennas to cover a wide frequency range. A method which can be applied to a broadband antenna using a long cable between the antenna and the LNA to eliminate the effect of the reflected LNA noise was developed by Rogers and Bowman [2008] but this method has significant limitations which will be discussed in section 8. Bowman and Rogers [2010] set a lower limit on the duration for the reionization epoch of $\Delta z > 0.06$ using a wideband spectrometer covering 100 to 200 MHz band. This limit corresponds to spectral width of only about 1 MHz because, lacking accurate calibration of the antenna mismatch, a polynomial fit whose degree increases dramatically with bandwidth is needed to remove the instrument response. The primary motivation for the method of calibration we explore in this paper is to extend the bandwidth over which a more sensitive search can be made for the very small 10–100 mK 21 cm line in the presence of the much stronger foreground of about 200–2000 K. A space probe with a wideband spectrometer [Burns *et al.*, 2012] placed in orbit around the moon is being studied for a mission to make observations of the red-shifted 21 cm line in the radio quiet zone on the far side of the moon. With the development of broadband antennas and spectrometers for astronomy, earth physics and other applications new methods are needed for accurate automated measurements over a wide frequency range. The sky noise power, T_{sky} , and

¹Haystack Observatory, Massachusetts Institute of Technology, Westford, Massachusetts, USA.

²School Of Earth and Space Exploration, Arizona State University, Tempe, Arizona, USA.

Corresponding author: A. E. E. Rogers, Haystack Observatory, Massachusetts Institute of Technology, Westford, MA 01886, USA. (arogers@haystack.mit.edu)

other quantities in this paper are a function of frequency but their frequency dependence is not explicitly indicated in equation (1) or in the mathematics that follows.

2. 50 ohm Measurements at a Fixed Reference Plane

[4] A vector network analyzer (VNA) provides an accurate measurement of the reflection coefficient referenced to the standard 50 ohm impedance and consequently it is convenient to use a VNA to measure both the antenna and receiver input reflection coefficient at the fixed reference plane defined by the 50 ohm connection between the receiver and the antenna. In this case, with some algebraic manipulation equation (1) becomes

$$T_{sky}(1 - |\Gamma|^2) = T_{sky}(1 - |\Gamma_a|^2)|F|^2 \quad (2)$$

where

$$\Gamma = \frac{Z_a - Z_l^*}{Z_a + Z_l} \quad (3)$$

$$F = \frac{(1 - |\Gamma_l|^2)^{1/2}}{1 - \Gamma_a \Gamma_l} \quad (4)$$

$$\Gamma_a = \frac{Z_a - 50}{Z_a + 50} \quad (5)$$

$$\Gamma_l = \frac{Z_l - 50}{Z_l + 50} \quad (6)$$

Z_a , Z_l and Γ_a , Γ_l are the impedances and reflection coefficients of the antenna and receiver respectively. Part of the complex factor F can also be viewed as the sum of the noise waves back and forth from the antenna to the receiver since the sum is a polylogarithmic series which converges when $|\Gamma_a \Gamma_l| < 1$ and has an exact solution

$$\sum_{i=0}^{\infty} (\Gamma_a \Gamma_l)^i = \frac{1}{1 - \Gamma_a \Gamma_l}. \quad (7)$$

[5] The LNA emits noise from its input which is reflected back from the antenna. This noise can be separated into a portion which is uncorrelated with the noise out of the LNA and another portion which is correlated with a portion of the LNA noise. The uncorrelated noise “wave” power depends only on the square of the magnitude of the antenna reflection while the correlated noise “wave” power depends on the magnitude and phase of the antenna reflection. We can add these receiver LNA noise waves to equation (2) to obtain the noise temperature, T_{rec} , from the LNA

$$T_{rec} = T_{sky}(1 - |\Gamma_a|^2)|F|^2 + T_u|\Gamma_a|^2|F|^2 + (T_c \cos(\phi) + T_s \sin(\phi))|\Gamma_a||F| + T_0 \quad (8)$$

where T_u is the uncorrelated portion of the LNA noise reflected from the antenna, T_c and T_s are the cosine and sine components of the noise from the LNA reflected by the

antenna which is correlated with the LNA output and T_0 is the portion of the noise which is independent of the LNA input. The noise reflected from the antenna reenters the LNA with phase, ϕ , which is equal to the phase of $\Gamma_a F$. Equation (8) is equivalent to the noise wave formulation of *Meys* [1978] if the “reference” impedance is that of the LNA in which case $F = 1$.

3. Receiver Calibration

[6] A three position switching sequence is used to provide the receiver calibration. A coax switch sequentially connects the LNA to the antenna and then to a 50 ohm ambient load and then while still connected to the load a calibrated noise source is turned on for the third state of the sequence. The uncalibrated noise power temperature in each position, P_{ant} , P_{load} , P_{cal} is

$$P_{ant} = gT_{rec} \quad (9)$$

$$P_{load} = g(GT_{amb} + T_0) \quad (10)$$

$$P_{cal} = g(G(T_{amb} + T_{cal}) + T_0) \quad (11)$$

where

$$G = 1 - |\Gamma_l|^2 \quad (12)$$

and g is the receiver gain, T_{amb} is the ambient temperature, and T_{cal} is the excess noise temperature of the calibration noise. The calibrated receiver output, T_{3p} , is

$$\begin{aligned} T_{3p} &= \frac{T_{cal}(P_{ant} - P_{load})}{(P_{cal} - P_{load})} + T_{amb} \\ &= T_{sky}(1 - |\Gamma_a|^2)|F|^2 G^{-1} \\ &\quad + T_u|\Gamma_a|^2|F|^2 G^{-1} \\ &\quad + (T_c \cos(\phi) + T_s \sin(\phi))|\Gamma_a||F|G^{-1} \end{aligned} \quad (13)$$

4. Measurement of LNA Noise Wave Parameters

[7] The LNA noise wave parameters, T_u , T_c and T_s can be measured by connecting an open (or shorted) low loss cable to the calibrated three-position switched spectrometer in place of the antenna. The cable acts just like an antenna looking at an isotropic sky with temperature equal to the cable’s physical temperature. The cable reflection coefficient, Γ_c , should be approximately

$$\Gamma_c = L_c \exp(-i\omega\tau_c) \quad (14)$$

where τ_c is the two-way delay, ω is the frequency in radians/s and L_c is the cable loss factor

$$L_c = 10^{-lc/10} \quad (15)$$

where lc is the one-way cable loss in dB. For highest accuracy the open cable’s reflection coefficient should be measured with the VNA since most cables are not exactly 50 ohms and the reflection coefficient is more complex than the expression above owing to the dispersion which results from the magnetic field within the skin depth of the

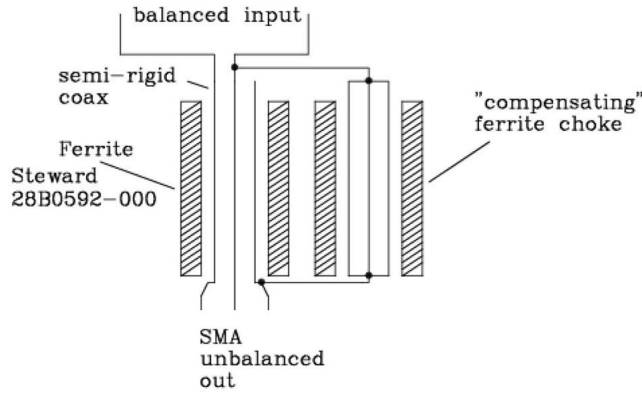


Figure 1. Ferrite choke balun.

conductors. This dispersion which becomes significant at low frequencies is analyzed in detail by *Ramo and Whinnery* [1953, chapter 6, section 6–10]. With the open cable connected the calibrated receiver output is given by equation (13) by substitution of T_{sky} and Γ_a with T_{amb} and Γ_c . Since the LNA noise parameters change gradually with frequency the rapid change of phase, ϕ , afforded by a cable of sufficient length allows the noise wave parameters to be separately estimated from the calibrated receiver output via a least squares fit to the functions $|\Gamma_a|^2|F|^2G^{-1}$, $\cos(\phi)|\Gamma_a||F|G^{-1}$ and $\sin(\phi)|\Gamma_a||F|G^{-1}$ after subtracting $T_{amb}(1 - |\Gamma_c|^2|F|^2)G^{-1}$. In an automated system it may be advantageous to use a compact mismatched circuit, as described by *Hu and Weinreb* [2004], instead of an open cable to measure the noise waves.

5. Corrections for Antenna Losses

[8] If the antenna is lossless the calibrated sky noise temperature can be obtained from equation (13)

$$T_{sky} = [T_{3p} - T_u|\Gamma_a|^2|F|^2G^{-1} - (T_c \cos(\phi) + T_s \sin(\phi))|\Gamma_a||F|G^{-1}] \times [(1 - |\Gamma_a|^2)|F|^2G^{-1}]^{-1} \quad (16)$$

noting that when $\Gamma_a = 0$, $T_{sky} = T_{3p}$.

[9] If the antenna loss factor, defined to be less than or equal to one and where one equals zero loss, is L the corrected sky temperature, T_{csky} , is

$$T_{csky} = (T_{usky} - T_{amb}(1 - L))/L \quad (17)$$

where T_{usky} is the uncorrected sky temperature and

$$L = 10^{-l/10} \quad (18)$$

where l is the loss in dB. For a typical antenna the loss is made of several components which include ground loss, resistive loss, transmission line loss and balun loss. The ground loss factor is one minus the fraction of the antenna pattern which receives thermal radiation from the ground. The resistive loss is one minus the fraction of the real part of the antenna impedance that comes from the conductor resistance including the skin effect. If a 50 ohm attenuator is

used between the LNA and the antenna the attenuator loss can be incorporated, taking into account the loss and thermal noise waves from both ends of the attenuator, so that equation (8) becomes

$$T_{rec} = T_{sky}(1 - |\Gamma_a|^2)|F|^2L_{att} + T_{amb}((1 - L_{att})L_{att}|\Gamma_a|^2 + 1 - L_{att})|F|^2 + T_u|\Gamma_a|^2|F|^2L_{att}^2 + (T_c \cos(\phi) + T_s \sin(\phi))|\Gamma_a||F|L_{att} + T_0 \quad (19)$$

where

$$F = \frac{(1 - |\Gamma_l|^2)^{1/2}}{1 - \Gamma_a\Gamma_lL_{att}} \quad (20)$$

and L_{att} is the loss factor of the attenuator.

6. Model for Choke Balun Loss

[10] The “choke” balun shown in Figure 1 is modeled by the circuit shown in Figure 2. In this model twice the ferrite impedance appears in parallel across the balanced antenna terminals so the reflection coefficient measured at the unbalanced port, Γ , is

$$\Gamma = L_{bc} \exp(-i\omega\tau_{bc})\Gamma_b \quad (21)$$

where Γ_b is the reflection coefficient of the antenna impedance Z_a , in parallel with Z_f which is twice the impedance of each individual ferrite choke. L_{bc} and τ_{bc} are the loss and two-way delay in the short cable, which is part of the balun, respectively. Z_b is given by

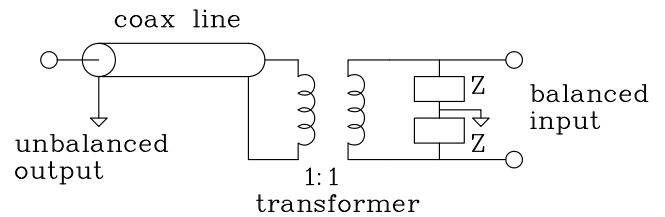
$$Z_b = 50 \left(\frac{1 + \Gamma_b}{1 - \Gamma_b} \right) \quad (22)$$

and Z_a is

$$Z_a = (1/Z_b - 1/Z_f)^{-1} \quad (23)$$

Since the noise power from impedance Z is proportional to its temperature times the real part of the impedance the loss factor is

$$L = \frac{\text{Re}(Z_a)|Z_f|^2}{(\text{Re}(Z_a)|Z_f|^2 + \text{Re}(Z_f)|Z_a|^2)} \quad (24)$$



Balun circuit model

Figure 2. Circuit model of ferrite choke balun.

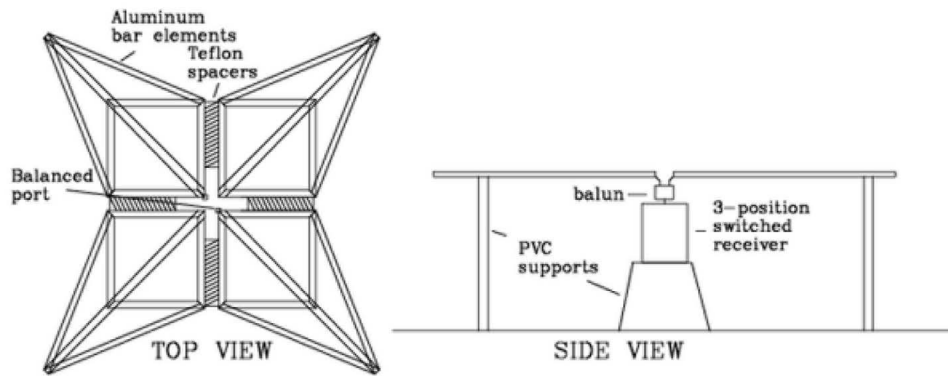


Figure 3. Fourpoint antenna 0.43λ tip-to-tip dipole 0.2λ above ground at 55 MHz.

The loss factor L can then be multiplied by the loss factor of the short cable which, after accounting for the antenna mismatch, is given by

$$L = L_{bc}(1 - |\Gamma|^2/L_{bc}^2)/(1 - |\Gamma|^2) \quad (25)$$

to obtain the overall loss factor for the balun. The phase shift through this short cable has already been taken into account by the antenna impedance measurement which is made with the balun included.

[11] The impedance Z_f can be measured by disconnecting the balun from the antenna and using the VNA to measure the reflection coefficient, Γ_{fopen} , of the balun open at the balanced antenna port so that

$$Z_f = 50 \left(\frac{1 + \Gamma_{fopen}(L_{bc})^{-1} \exp(i\omega\tau_{bc})}{1 - \Gamma_{fopen}(L_{bc})^{-1} \exp(i\omega\tau_{bc})} \right) \quad (26)$$

where $(L_{bc})^{-1} \exp(i\omega\tau_{bc})$ corrects for the loss and delay of the short cable in the balun. The small loss in this cable and its delay are measured separately from the reflection coefficient, Γ_{fshort} of the balun with the balanced output shorted. Equivalently, the open and shorted measurements can be used to obtain Z_f directly

$$Z_f = 50 \left(\frac{1 + \Gamma_{fopen}\Gamma_{fshort}^{-1}}{1 - \Gamma_{fopen}\Gamma_{fshort}^{-1}} \right). \quad (27)$$

7. Example of Calibrated Sky Spectrum Measurement From 55 to 110 MHz

[12] A short observation of the sky spectrum was made with a broadband dipole and a three-position switched spectrometer at a remote site away from strong TV and FM radio signals to test the calibration method. The switched spectrometer made the measurements of the following: (1) 50 ohm resistor heated to 100 K above ambient, (2) an open cable about 3 m in length, and (3) sky noise at the remote site. VNA reflection coefficient (S11) measurements were made of the following: (1) antenna through the balun at the remote site, (2) input of the LNA through the three-position switch, (3) open cable used to derive the LNA noise parameters, and (4) open and shorted balun to measure balun ferrite choke impedance.

[13] Measurements of the heated resistor were used to calibrate the internal noise diode in flatness and absolute scale. Following this calibration, measurements of the heated load had a RMS deviation from a constant under ~ 20 mK. For a heated load we chose a noninductive 50 ohm resistor with 1% tolerance and 50 ppm temperature coefficient to maintain a reflection coefficient better than -46 dB. With the short path length from the load to the LNA this reflection coefficient is sufficient to maintain spectral flatness at the mK level in the 50–200 MHz frequency range. If necessary the mismatch can be calibrated in this frequency range using accurate measurements of the DC resistance of the load over the temperature range used for the measurements. To remove any uncertainty in the temperature of this “hot” the measurement was checked using a HP346C noise source with calibration traceable to the National Institute of Standards and Technology (NIST). We note however that the absolute temperature scale is not as critical as the spectral flatness.

[14] The wideband dipole used for the test is based on the “Fourpoint” design of *Suh et al.* [2004]. This antenna which was made of aluminum rod elements instead of panels is shown in Figure 3. Figure 4 shows a block diagram of the system used to measure the sky noise spectrum which includes the antenna, balun, three-position switch, LNA and spectrometer. It also shows a noise source used to inject added noise below 55 MHz which conditions the analog to digital converter (ADC). This “out of band” conditioning improves the linearity and dynamic range of the ADC needed for accurate cancelation of the receiver gain, g , and constant, T_0 , for the calibrated receiver output, T_{3p} , given in equation (13).

[15] Figure 5 shows the measured reflection magnitude and phase along with a Fourier series least squares fit to the data to reduce the noise in the VNA data and provide accurate interpolation between measurements. The RMS difference between the polynomial fit and the VNA data is 0.05 dB in magnitude and 0.4° in phase.

[16] Figure 6 shows the measured reflection coefficient of the LNA. In this case the value of fitting a Fourier series is clearly evident as the VNA measurements of the LNA were made with a spacing of 10 MHz to reduce the noise in the measurements because the VNA output had to be set to a low enough level to avoid saturating the LNA. The RMS difference between the fit and the VNA data is 0.2 dB in

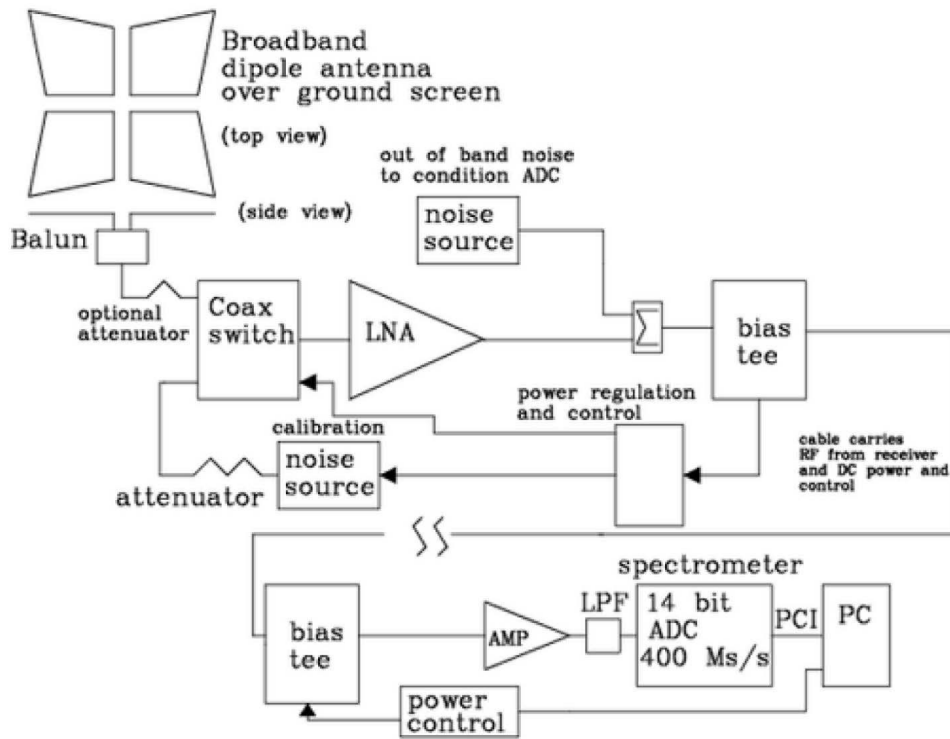


Figure 4. Block diagram of complete system for sky noise measurements. The “three-position” switch sequence is implemented with a 50 ohm coax switch which connects the LNA to the antenna and then to an ambient load, formed by a 30 dB attenuator, and then the noise source is turned on to provide the calibration.

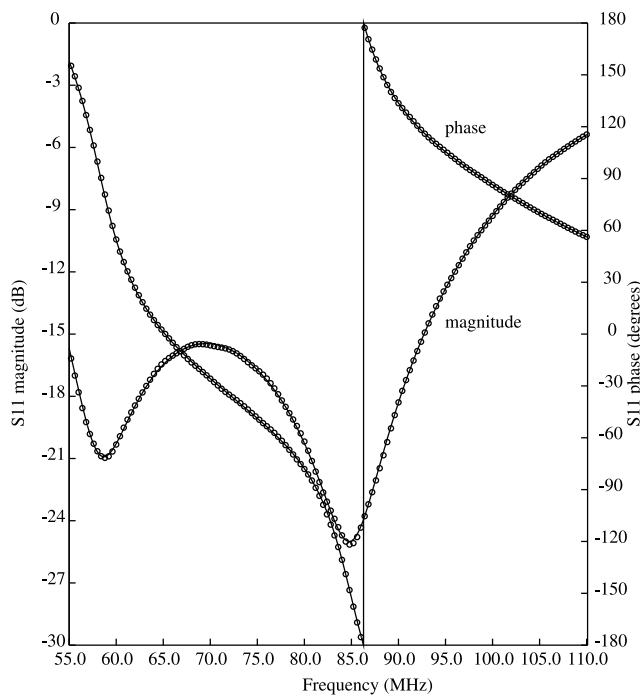


Figure 5. Antenna reflection coefficient, Γ_a , measurements with best fit Fourier series of eight complex coefficients plus a constant. The RMS difference between the polynomial fit and the VNA data is 0.05 dB in magnitude and 0.4° in phase.

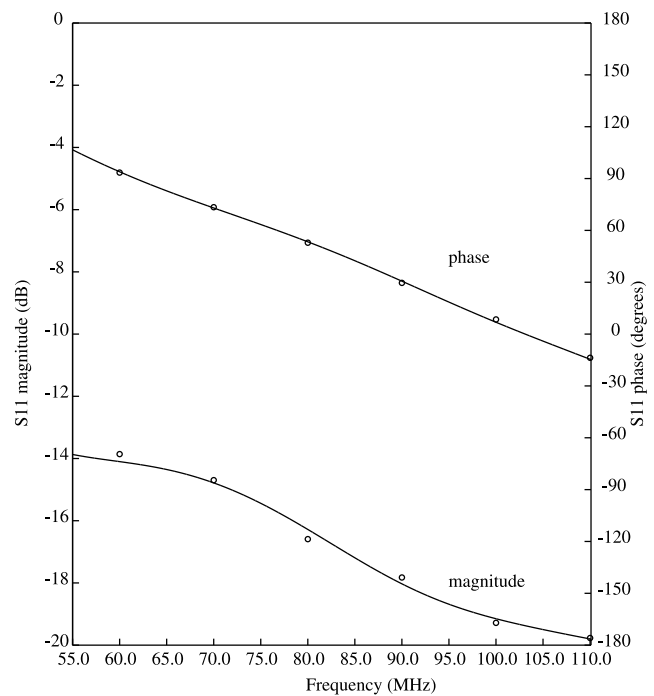


Figure 6. LNA reflection coefficient, Γ_b , measurements with best fit Fourier series of four complex coefficients plus a constant. The RMS difference between the polynomial fit and the VNA data is 0.2 dB in magnitude and 1.1° in phase.

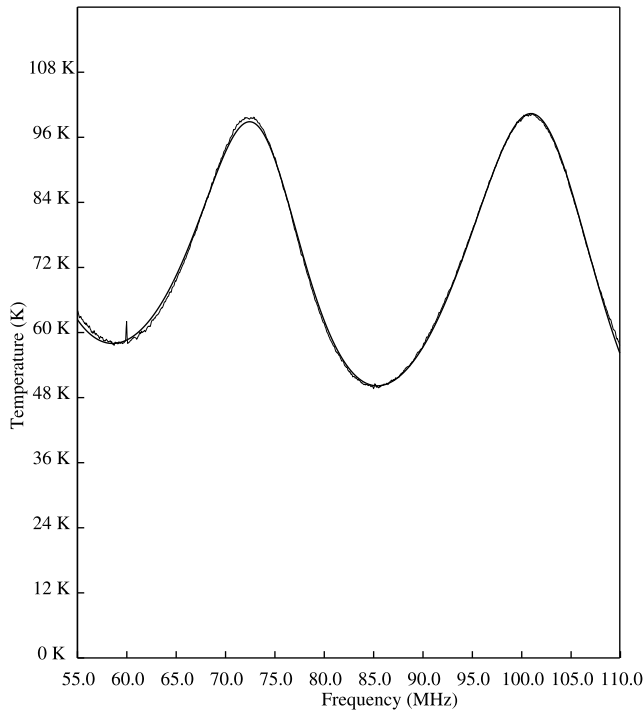


Figure 7. Spectrum of open cable with best fit curve from the LNA noise parameters plotted in Figure 8. The RMS difference between the fit and the spectrum is 0.6° .

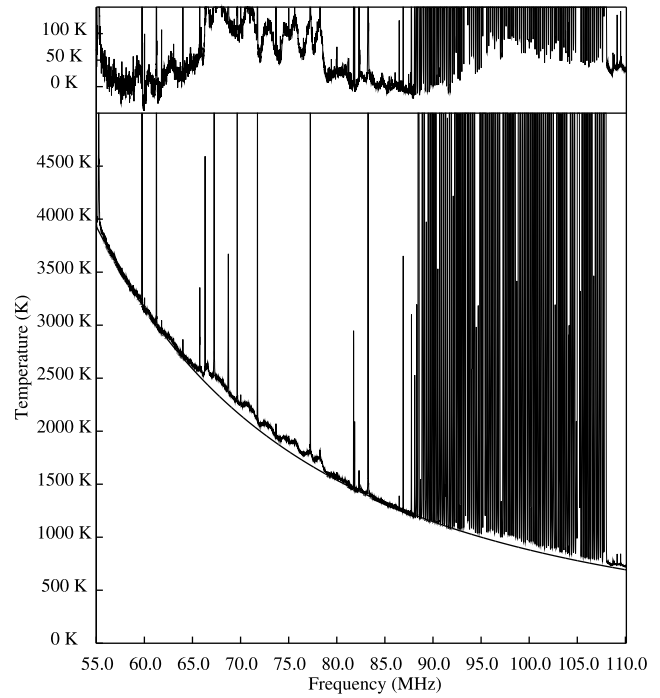


Figure 9. Calibrated sky noise spectrum without attenuation with best fit spectral index. The spikes and portions of the calibrated spectrum extending above the best fit sky noise spectrum are contaminated with interference and have been excluded from the least squares fit. Channels included in the fit are plotted with thicker lines. The difference between the observed spectrum and the best fit is shown with an expanded scale at the top.

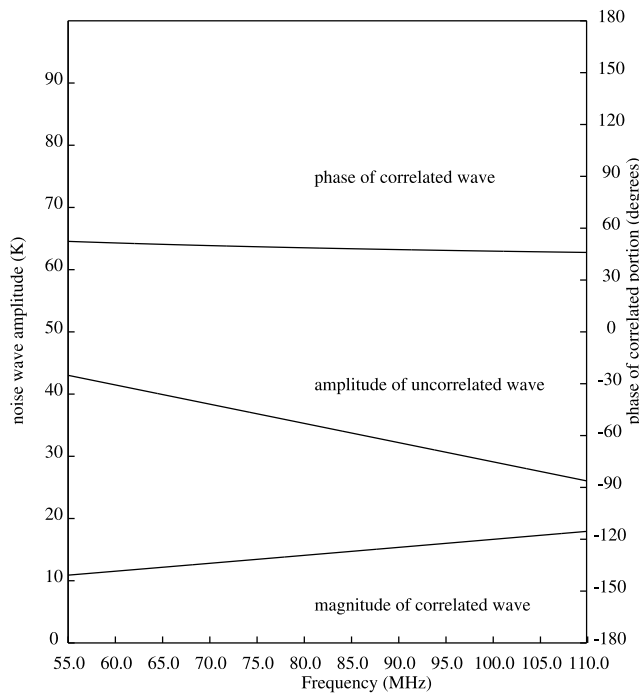


Figure 8. LNA noise parameters. Top curve is the phase ($\tan^{-1}(T_s/T_c)$) of the correlated noise. The middle curve is uncorrelated noise, T_u , and the bottom curve is the magnitude ($(T_s^2 + T_c^2)^{1/2}$) of the correlated noise.

magnitude and 1.1° in phase. A more capable VNA and longer averaging will be employed in the future.

[17] Figure 7 shows the spectrum of the calibrated three-position switched spectrometer connected to the open cable with two-way delay of 29 ns and a two-way loss of 0.5 dB at 50 MHz increasing with the square root of frequency to 0.7 dB at 100 MHz. The solid curve is the spectrum derived from the best fit LNA noise parameters shown in Figure 8. The RMS difference between the polynomial fit and the spectrum is 0.6 K. The frequency dependence of the noise parameters were constrained to a constant plus a slope. At 80 MHz the values of T_u , T_c , T_s were 35, 9, and 10 K respectively.

[18] Figures 9 and 10 show the calibrated sky spectrum for 2 sequential observations of about 10 min each taken at the remote site in West Forks, Maine on 8 July 2011 at 17:05 and 17:20 UT respectively. In the first the antenna was connected directly to the three-position switch and in the second the antenna was connected through a 6 dB attenuator. These calibrated spectra were derived using equation (16) or from equation (19), in the case of the use of the added attenuation, followed by equation (17) for the correction of the antenna, balun cable and balun ferrite loss factors. The balun ferrite loss factor was calculated using equation (24) using a value for twice the ferrite choke impedance which varied from $815 + 194j$ ohms at 50 MHz to $780 - 155j$ ohms at 100 MHz from VNA measurements of the balun open at

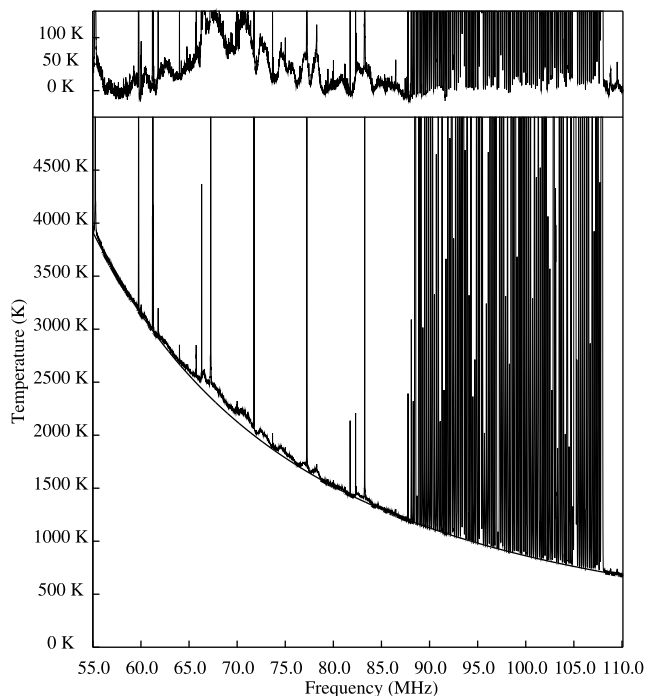


Figure 10. Calibrated sky noise spectrum and best fit spectral index from measurements made with 6 dB attenuation. The major sources of interference are FM (88–108 MHz) and digital TV channel 4 (66–72 MHz). The difference between the observed spectrum and the best fit is shown with an expanded scale at the top.

the antenna end converted to impedance using equation (26). Substitution of these impedance values into the circuit model, and including the very small loss (~ 0.01 dB) in the short coax cable within each balun, gives a balun one-way loss of 0.265 dB and 0.28 dB at 50 and 100 MHz respectively and is consistent with measurements of back-to-back baluns made as a check. The balun common mode rejection (CMRR) was measured and found to be better than 45 dB from 50 to 110 MHz. This measurement was made using a signal generator and dual channel oscilloscope with each channel terminated in 25 ohm resistors to measure the ratio of the common to differential modes by adding and then subtracting the traces. Electromagnetic simulations were used to show that a CMRR of over 45 dB provides sufficient rejection of the vertically polarized response of the common mode of the dipole to have an effect of less than 0.02 dBi on the antenna pattern for elevations above 5° . A loss factor of 0.93 was assumed for the ground loss of 7% based on the results of an electromagnetic simulation of the antenna and ground plane. The effect of the CMRR on the ground loss was estimated to be less than 1%. The overall loss factor is the product of the balun and ground loss factors. The antenna was assumed to have no significant resistive loss.

8. Determination of Spectral Index

[19] An estimate of the spectral index is obtained by finding the function,

$$T_{sky}(f) = T_{sky}(f_r)(f/f_r)^{-sp} \quad (28)$$

where $T_{sky}(f)$ is the sky temperature as a function of frequency f , sp is the spectral index and f_r is the “reference” frequency that fits the calibrated sky noise spectrum using weighted least squares for which portions of the spectrum with added interference are given zero weight. The best fit spectral indices using the calibrated sky spectra shown in Figures 9 and 10 were 2.50 ± 0.05 and 2.53 ± 0.05 respectively. While the difference is within the errors the data without attenuation could have been effected by non linearity in the ADC owing to high level of interference. These values are in good agreement with measurements made from 100 to 200 MHz by *Rogers and Bowman* [2008] in which the LNA was connected to the antenna via a long cable so that correlated noise terms are fitted and removed from the sky noise spectrum. The disadvantage of this method is the added loss in the long cable used to provide the rapid change of phase of the reflection coefficient. In addition the “ripples” in the measured spectrum are assumed to arise only from the mismatch and cannot be separated from fine-scale structure which might be present in the sky spectrum. In this method the antenna reflection coefficient was measured by injecting added noise which was then reflected by the antenna and measured by the spectrometer. However, the antenna reflection coefficient could have been measured with a VNA. The measurement of spectral index was only intended as a short test of the calibration at the site in Maine which is a few hours drive from the M.I.T. Haystack observatory. The results, as can be seen from the spectra in Figures 9 and 10, are contaminated by significant interference and in addition the data was taken in the daytime when the radiation from the sun and absorption in the ionosphere could have an influence on the results.

9. Sensitivity of Calibration to Ancillary Measurement Errors

[20] When the sky noise dominates 2 terms in equation (19) determine the error in sky temperature. The first, $(1 - |\Gamma_a|^2)$, results in an error of $2|\Gamma_a|^2 T_{sky}$ times the error in reflection magnitude and the second, $(1 - \Gamma_a \Gamma_l L_{att})$, results in an error of $|\Gamma_a| |\Gamma_l| T_{sky} L_{att}$ times the error in reflection magnitude. The second term is also dependent on errors in the phase of the reflection phase. The error which results from this second term becomes less significant for larger values of attenuation.

[21] For the particular case of the test observations the sensitivity to measurement errors in the ancillary measurement of antenna and LNA reflection coefficient, balun ferrite impedance and ambient temperature was determined by using equation (19) to generate noiseless “reference” data assuming a sky temperature of 1500 K at 80 MHz and a spectral index of 2.5. New simulated data was then generated by perturbing the ancillary VNA data, first by 1% in amplitude, and then by 0.01 radians in phase for parameters listed in Table 1. A test of the sensitivity to the ambient temperature was made by changing the ambient temperature by 1 K. These two data sets were then processed to obtain the calibrated sky temperature and after removing the best fit spectral index plus a constant their RMS differences computed. The results with an attenuator of 10 dB placed between the antenna and the three-position switch are given in Table 1. The largest error in spectral index occurred for a

Table 1. Sensitivity to Changes in Ancillary Measurements Obtained From Simulations in Which Each Parameter Was Changed by 1% in Amplitude and 0.01 Radians of Phase^a

Parameter Changed	RMS (K)	rms2 ^b (K)
Γ_a amplitude	1.3	0.02
Γ_a phase	0.1	0.02
Γ_l amplitude	0.1	0.02
Γ_l phase	0.16	0.01
Z_f amplitude	0.34	0.02
Z_f phase	0.04	0.02
T_{amb} temperature	0.7	0.01

^aThe sensitivity to ambient temperature is given for a change of 1 K.

^brms2 is for antenna with -20 dB reflection coefficient.

1% change in the antenna reflection amplitude for which the best fit value was -2.492 . In all other cases the change in spectral index was less than 0.001. The RMS values of the systematic residuals in Table 1 are a measure of the accuracy in the ancillary measurements needed to set new limits on the deviations in the sky noise spectrum due to the redshifted 21 cm line. A major conclusion is that an antenna reflection coefficient better than about -20 dB over a wide bandwidth is needed to avoid systematic errors from the errors in measurement of its reflection coefficient as a 1% in amplitude (0.1 dB) is close to the limit of accuracy expected from a well calibrated VNA. The sky noise tests described in the previous section are not good enough to determine the limits of this new method so tests using a hot load with intentional mismatch are being made in the laboratory to determine the calibration accuracy under controlled conditions without interference. These laboratory tests combined with long integrations at a site with lower levels of interference will be needed to determine the practical limits. In addition, an accurate model for the effects of the antenna beam shape, and antenna loss will be needed.

[22] For long integrations in which the systematics still dominate an attenuation of about 10 dB is optimum for the high sky noise temperature at 80 MHz. The effect of attenuation is to reduce the sensitivity to errors in the measurement of the phase of the antenna reflection coefficient as well as errors in the reflection coefficient of the LNA but does not reduce the sensitivity to errors in the amplitude of the antenna reflection coefficient which in the limit becomes $2|\Gamma_a|^2 T_{sky}$ times the error in reflection coefficient magnitude. This limit equals about 300 mK for -20 dB reflection, 1% error in reflection coefficient and 1500 K sky temperature. Using more attenuation makes little difference to the sensitivity to errors in the ancillary measurements and without an attenuator the sensitivity to error in the reflection coefficients for the antenna used in this test is increased by about a factor of 2. It is noted that the most critical measurement is that of the antenna impedance. However, the sensitivity to antenna impedance can be reduced if an antenna with a better match over the wide frequency range can be obtained. For example a large reduction in sensitivity could be obtained with an antenna whose reflection coefficient is below -20 dB from 55 to 110 MHz as shown by the numbers in the last column of Table 1. A reduction of the sensitivity to antenna reflection coefficient by a factor of about 3 can be obtained with the “Fourpoint” used in the test if the frequency range is limited to 60 to 90 MHz. We also note the large sensitivity to the balun and designs with lower loss are being studied. In

order to increase the accuracy of the ancillary measurements it may be better to use an impedance analyzer instead of a VNA as this instrument can achieve higher accuracy than a VNA in the frequency range below 110 MHz.

[23] Special care is needed for the measurements of antenna impedance since the impedance is affected by structures close to the antenna. For highest accuracy the measurements need to be made using a metal structure with the same dimensions as the receiver. Also the antenna impedance changes with temperature, due to the expansion of the antenna, and with refractivity changes in the surrounding atmosphere. An estimate of the effect of a temperature change, based on the expansion coefficient of the antenna, is of the order of 0.1% for a 20 K change in temperature. The refractivity of air at sea level is about 300 N units (refractivity = 1.0003) and varies by about 100 N units with changes in humidity. It is estimated that a change in refractivity of 100 N units will change the antenna impedance by about 0.01% and consequently it may be necessary to record ground level refractivity in addition to temperature and make corrections based on the coefficients of sensitivity to temperature and refractivity. In addition corrections may be needed for the changes in the LNA and balun unless their temperature is controlled. With some added complexity the VNA or impedance analyzer could be connected with coax switches to allow periodic measurements to be made automatically. Finally, a sufficiently large ground plane is required to reduce the effects of changes in the surrounding ground to a negligible level for the highest accuracy.

10. Conclusion

[24] The accurate calibration method described has the potential to make wideband sky noise spectral measurements with greatly reduced level of systematics. Simulations of performance indicate that in order to reach a level of 20 mK an antenna reflection coefficient better than about -20 dB is needed to avoid being limited by the accuracy the antenna reflection coefficient measurement using a vector network analyzer.

[25] **Acknowledgment.** We thank Delani Cele of Ithaca College, New York, who made the antenna and balun VNA measurements and helped with the setup of the dipole at West Forks, Maine, while he spent the summer of 2011 at Haystack Observatory under the NSF-supported Research Experiences for Undergraduates (REU) program.

References

- Bowman, J. D., and A. E. E. Rogers (2010), A lower limit of $\Delta z > 0.06$ for the duration of the reionization epoch, *Nature*, 468, 796–797.
- Burns, J. O., J. Lazio, S. Bale, J. Bowman, R. Bradley, C. Carilli, S. Furlanetto, G. Harker, A. Loeb, and J. Pritchard (2012), Probing the first stars and black holes in the early universe with the Dark Ages Radio Explorer (DARE), *Adv. Space Res.*, 49(3), 433–450.
- Furlanetto, S. R., S. P. Oh, and F. H. Briggs (2006), Cosmology at low frequencies: The 21 cm transition and the high-redshift universe, *Phys. Rep.*, 433, 181–301.
- Gnedin, N. Y., and P. A. Shaver (2004), Redshifted 21 centimeter emission from the pre-reionization era I. Mean signal and linear fluctuations, *Astrophys. J.*, 608, 611–621.
- Hargreaves, J. K., and D. L. Detrick (2002), Application of polar cap absorption events to the calibration of riometer systems, *Radio Sci.*, 37(3), 1035, doi:10.1029/2001RS002465.
- Hu, R., and S. Weinreb (2004), A novel wide-band noise-parameter measurement method and its cryogenic application, *IEEE Trans. Microwave Theory Tech.*, 52(5), 1498–1507.

- Meys, R. P. (1978), A wave approach to the noise properties of linear microwave devices, *IEEE Trans. Microwave Theory Tech.*, 26, 34–37.
- Pauliny-Toth, I. K., and J. R. Shakeshaft (1962), A survey of the background radiation at a frequency of 404 Mc/s, *Mon. Not. R. Astron. Soc.*, 124, 61–77.
- Ramo, S., and J. R. Whinnery (1953), *Fields and Waves in Modern Radio*, John Wiley, New York.
- Rogers, A. E. E., and J. D. Bowman (2008), Spectral index of the diffuse radio background measured from 100 to 200 MHz, *Astron. J.*, 136, 641–648.
- Shaver, P. A., R. A. Windhorst, P. Madau, and A. G. de Bruyn (1999), Can the reionization epoch be detected as a global signature in the cosmic background?, *Astron. Astrophys.*, 345, 380–390.
- Suh, S.-Y., W. Stutzman, W. Davis, A. Waltho, K. Skeba, and J. Schiffer (2004), A novel low-profile, dual-polarization, multi-band base-station antenna element the fourpoint antenna, paper presented at Vehicular Technology Conference, Inst. of Electr. and Electron. Eng., Los Angeles, Calif.
- Turtle, A. J., J. F. Pugh, S. Kenderdine, and I. I. K. Pauliny-Toth (1962), The spectrum of the galactic radio emission: I. Observations of low resolving power, *Mon. Not. R. Astron. Soc.*, 124, 297–312.